ELSEVIER

Chemical Engineering Journal 91 (2003) 45–58

Chemical Engineering Journal

www.elsevier.com/locate/cej

Effect of thermolysis on resid droplet vaporization in fluid catalytic cracking

Z. Huang[1], T.C. Ho*

Corporate Strategic Research Labs, ExxonMobil Research and Engineering Company, Annandale, NJ 08801, USA

Received 30 October 2001; accepted 11 May 2002

Abstract

Heavy feed cracking is certain to play an increasingly important role in oil refining. Against this backdrop, this work aims to gain some understanding of how thermolysis affects the manner in which a heavy Arabian vacuum resid droplet vaporizes in fluid catalytic cracking (FCC). Specifically, we study the vaporization history of the droplet under two limiting conditions that bracket the actual vaporization process. One is a high-temperature environment in which the catalyst heats up only the resid droplet. Another is a low-temperature environment in which the catalyst vaporizes a gas oil before heating the resid droplet. Key findings are as follows: (1) Droplet life can go through one, two, or three stages, depending on the drop size and environment. A large droplet in the high-temperature environment goes through the heat-up, thermolysis and evaporation stages. A small droplet at low temperatures goes through only the heat-up stage. (2) The effect of thermolysis increases with temperature and the initial drop size. (3) Thermolysis can significantly lower the drop's steady-state temperature—the larger the drop, the greater the effect and, hence, the longer the drop lifetime and (4). During the evaporation stage, the drop's surface area decrease can be approximated by the classical D^2-law.

Keywords: Fluid catalytic cracking; Droplet vaporization; Thermal cracking; Heavy oils vaporization

1. Introduction

Fluid catalytic cracking (FCC) has been, and will remain for quite some time, the primary conversion process in oil refining [1]. In a typical present-day FCC process, a liquid feed mixture is atomized through a nozzle to form small droplets at the bottom of an FCC riser. The droplets contact hot regenerated catalyst and are vaporized and cracked to lighter products and coke. The vaporized products rise through the riser. The catalyst is separated out from the hydrocarbon stream through cyclones. Once separated, the catalyst is stripped in a steam stripper of adsorbed hydrocarbons and then fed to a regenerator, where coke is burnt off. The products are sent to a distillation column for fractionation into selected products (light olefins, gasoline, diesel, etc.). The catalyst, once regenerated, is then fed back into the riser to complete the circuit.

With today's high-activity FCC catalysts, the majority of the cracking and catalyst coking occur in the vicinity of the feed injection zone. As the need to crack more and heavier hydrocarbons at ever shorter contact times grows, oil droplet vaporization may become rate limiting in FCC. A fast vaporization is highly desirable because vapor-phase cracking is faster and more selective than liquid-phase cracking. While the combustion literature abounds with both theoretical and experimental works on droplet vaporization, such is not the case with FCC. The few theoretical studies of FCC feed vaporization have focused on relatively light hydrocarbons [2–7] that boil below 1050 °F, the final nominal boiling point of gas oils. All those studies invoke a reasonable assumption that thermal cracking is unimportant during the vaporization process. As such, the process is essentially characterized by two stages: heat-up followed by evaporation.

By their very nature, heavy feeds (with initial boiling point above 1050 °F) are more difficult to vaporize and more thermally crackable than gas oils (650–1050 °F nominal boiling range). There are other complicating factors that can prolong the vaporization time of heavy oil drops. One is that thermolysis may exert an appreciable cooling effect due to reaction endothermicity. Another factor is that heavy oils tend to form large drops because they are hard to atomize. Still another is that the refiner may have to lower the feed temperature to limit the regenerator temperature rise caused by the high coke-forming tendency of heavy oils.

* Corresponding author.
E-mail address: teh.c.ho@exxonmobil.com (T.C. Ho).
[1] Present address: Foster Wheeler USA Corporation, 2020 Dairy Ashford Road, Houston, TX 77077, USA.

1385-8947/02/$ – see front matter
PII: S1385-8947(02)00114-6

Nomenclature

A	riser cross-sectional area
B	evaporation constant in the D^2-law
C_{pc}, C_{pd}	heat capacities of catalyst and resid droplet, respectively
C_{po}, C_{ps}	heat capacities of hydrocarbon vapor and steam, respectively
C_{pl}, C_{pg}	heat capacities of liquid gas oil and gas (gas oil or steam), respectively
D	average diameters of resid droplet at time t
D_e	average diameters of resid droplet at thermal equilibrium
D_f	average diameter of resid feed droplet ($t = 0$)
D_{rg}	resid component diffusivity
E_i	activation energy for resid thermal cracking (50 kcal/mol for every i)
F_c	mass flow rate of catalyst
F_v, F_{vi}	mass flow rates of resid vapor and of ith resid component in the vapor
F_f, F_o	mass flow rates of liquid resid feed and of total hydrocarbon vapor
F_s, F_{tf}	mass flow rates of steam and of total hydrocarbon feedstock in the feed
F_g, F_{gf}	mass flow rates of vapor gas oil and of feed gas oil vapor, respectively
ΔH_c	heat of resid thermal cracking
ΔH_{gv}	vaporization heat of gas oil
ΔH_{vi}	heat of resid vaporization
k_i	thermal cracking rate constant for ith resid boiling fraction
k_e	resid vapor-liquid equilibrium constant
k_g, k_o	heat conductivities of gas and gas oil vapor, respectively
k_s	steam heat conductivity
k_x	mass transfer coefficient
M_i	average molecular weight of the ith resid boiling fraction (Table 2)
M_{go}	average molecular weight of gas oil (300 kg/kmol)
P_{rb}	pressure at riser bottom
R_{co}	catalyst to oil, F_c/F_{tf}
r_{ci}	thermal cracking rate of ith resid boiling fraction
r_{vi}	evaporation rate of ith resid boiling fraction
T	temperature of resid droplet
T_{bi}	average normal boiling point for the ith boiling fraction
T_{bp}	bubble point
T_f, T_{gf}	temperatures of resid and gas oil in the feed, respectively
T_g	temperature of gas oil in the gas phase
T_{rg}	temperature of regenerated catalyst
T_s	feed steam temperature at riser bottom
v	slip velocity $v = u_g - u_d$, where u_g and u_d are gas and drop velocities, respectively
v_t	terminal velocity
W, W_f	masses of resid droplet at time t and $t = 0$, respectively
W_i	mass of ith resid component in resid droplet at time t
x_i	mass ratio defined as $x_i = W_i / W_f$
x_{vi}	mass ratio defined as $x_{vi} = F_{vi} / F_{tf}$
x_{df}	mass ratio defined as $x_{df} = F_f / F_{tf}$
x_{if}	x_i at time $t = 0$
x_o	mass ratio defined as $x_o = F_o / F_{tf}$
x_s	mass ratio defined as $x_s = F_s / F_{tf}$
y_i	mole fraction of the ith resid component in the vapor phase

Greek letters

α_o	relative flow rate of oil vapor
α_s	relative flow rate of steam
ε	riser void fraction
μ_g, μ_o, μ_s	viscosities of gas, oil vapor, and steam
ρ_c, ρ_d, ρ_i	densities of catalyst, resid drop, and resid component i
ρ_g, ρ_o, ρ_s	densities of gas, oil vapor, and steam

The present study is motivated by the expectation that the importance of thermolysis may rival that of evaporation in heavy feed FCC and, therefore, should be given due consideration. Accordingly, our intent here is to gain some understanding of how thermolysis affects the manner in which a heavy Arabian vacuum resid droplet vaporizes. We do so by developing a most elementary theory that captures the salient features of the interplay of interfacial heat/mass transfer, thermolysis, and gas-drop slip. To this end, we dissect the problem into two simpler pieces by considering two limiting cases that bracket the actual vaporization process in resid FCC. Case A is a high-temperature environment in which all the heat contained in the catalyst is used to heat up the resid droplet. Case B is a low-temperature environment in which the catalyst first vaporizes a gas oil and then heats up the resid droplet. In addition to improving fundamental understanding, the results should have a bearing on split feed injection. For instance, Case A corresponds to a configuration, where the injection of the resid feed is made upstream of that of the gas oil feed.

Before proceeding further, it is useful, for perspective, to briefly describe the earliest theory of droplet evaporation [8]. It considers a pure-component spherical drop evaporating into a quiescent gas at constant temperature. The theory posits that the decrease in the droplet diameter D changes very slowly with time t as evaporation proceeds.

After initial transients, the system reaches a steady state that the heat needed to evaporate the liquid and to heat up the vapor to the surrounding gas temperature is exactly balanced by the sensible heat transferring from the gas to the droplet. The liquid and its vapor are at equilibrium at the interface. These assumptions lead to the classical D^2-law: $D_f^2 - D^2(t) = Bt$ where D_f and $D(t)$ are, respectively, the droplet diameter at time zero and time t, whereas B is referred to as the evaporation constant. The D^2-law, which has been verified experimentally, can also be shown to hold true for droplet evaporation with Stefan flow and for burning droplets [8]. We shall examine the relevance of the D^2-law to the problem addressed here.

2. Model development

Let us first give a qualitative picture of the events underlying the model. The freshly regenerated catalyst at temperature T_{rg} instantaneously reaches thermal equilibrium with steam in Case A or with gas oil and steam in Case B. The liquid atomization process takes place instantaneously at the nozzle exit. The liquid spray is so dilute that the droplets would not perturb the gas velocity field and that the interactions among droplets are negligible. We thus consider an isolated, initially cold spherical drop comprising six boiling fractions of different thermal reactivities. During its flight toward the riser top, the droplet receives heat from the flowing gas. Once sufficiently heated, the droplet's size starts to shrink due to simultaneous thermolysis and evaporation.

Other major simplifying assumptions are as follows: (1) The cooling rates of the catalyst and of the gas are much slower than the heating rate of the resid droplet; that is, the catalyst and gas are at quasi-steady state during droplet heat-up. (2) The composition and temperature within the droplet are spatially uniform but temporally varying (see Appendix A for justification); that is, the vaporization process resembles that of batch distillation. (3) Heat transfers by radiation and natural convection are negligible. (4) The effect of curvature on vapor pressure is insignificant. (5) Momentum transfer is much faster than heat transfer, so the droplet quickly decelerates to its terminal velocity prior to appreciable heating. (6) The evaporation is so slow that the radial convective flow (Stefan flow) is negligible. (7) Thermophysical parameters are constants. (8) The products of resid thermolyis are gas oils; thermal coke, formed from secondary condensation reactions, can be neglected. (9) Gas oil does not crack thermally under the conditions studied [9].

In what follows, we develop the conservation equations governing sensible heating, evaporation and thermolysis. To complete the problem statement, we then present constitutive relations and correlations. The equations marked with an asterisk are the final model equations.

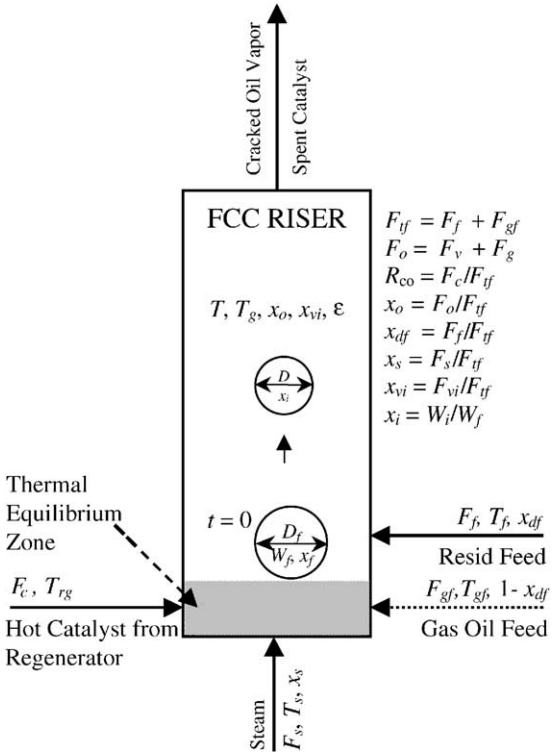

Fig. 1. Schematic diagram of resid droplet vaporization model: the three solid arrows represent feed streams for Case A; for Case B, the oil feed stream also contains gas oil as represented by the dotted arrow.

2.1. Mass balance

Referring to Fig. 1, let the mass flow rates of the catalyst, steam, liquid resid feed, vapor resid, vapor gas oil, total hydrocarbon (resid + gas oil) in the feed, and total hydrocarbon (resid + gas oil) vapor be F_c, F_s, F_f, F_v, F_g, F_{tf}, and F_o, respectively. At $t = 0$, $F_v = 0$ and $F_g = F_{gf}\ \delta$, where $\delta = 0$ for Case A and $\delta = 1$ for Case B. Also, $F_{tf} = F_f + F_{gf}$. At any time t, $F_o = F_g + F_v$. The following equation, in the Lagrangian fashion, tracks the loss of the ith boiling fraction in the droplet due to evaporative mass transfer and thermolysis:

$$\frac{d(W_f x_i)}{dt} = -r_{vi} - r_{ci}, \quad i = 1, 2, \ldots, 6 \qquad (1^*)$$

Here W_f is the drop's initial mass (the subscript f refers to the feed) and $x_i \equiv W_i / W_f$, where W_i is the mass of the ith boiling fraction in the resid drop at time (of flight) t. The evaporation rate r_{vi} and the thermolysis rate r_{ci} are both first order in x_i, whose expressions are given later. Evidently, a major objective of this study was to assess the relative importance of thermolysis versus evaporation. As a result of evaporation, there is an increase in the resid concentration in the vapor phase; that is,

$$\frac{dx_{vi}}{dt} = \frac{x_{df}}{W_f} r_{vi} \qquad (2^*)$$

where x_{vi} is the ratio of the mass flow rate of ith boiling fraction in the vapor phase (F_{vi}) to that of the total feedstock (F_{tf}) and $x_{df} = F_f/F_{tf}$, as shown in Fig. 1. Note that $F_v = \sum_i F_{vi}$. At $t = 0$, $x_{vi} = 0$. We can also write the mass balance equation for the total hydrocarbon concentration in the vapor phase,

$$\frac{dx_o}{dt} = -x_{df}\sum_i \frac{dx_i}{dt} \tag{3*}$$

with $x_o = F_o/F_{tf}$. At $t = 0$, $x_o = (1 - x_{df})\delta$. We next consider energy balance.

2.2. Energy balance

As assumed earlier, the hot catalyst instantaneously reaches the thermal equilibrium temperature T_g with steam in Case A or with gas oil and steam in Case B. The overall heat balance is described as follows by

$$\frac{d}{dt}[(F_c C_{pc} + F_s C_{ps} + F_o C_{po})T_g] = -\frac{F_f}{W_f}\frac{d}{dt}\left(W_f C_{pd} T \sum_i x_i\right) - F_f(C_{po} - C_{pd})T\sum_i \frac{dx_i}{dt} \tag{4}$$

in which the heat capacities of vapor resid and vapor gas oil are assumed to be the same. By virtue of Eq. (3), Eq. (4) can be simplified to

$$\frac{dT_g}{dt} = -\frac{x_{df}}{R_{co}C_{pc} + x_s C_{ps} + x_o C_{po}} \times \left[C_{pd}\sum_i x_i \frac{dT}{dt} - C_{po}(T_g - T)\sum_i \frac{dx_i}{dt}\right] \tag{5*}$$

with $R_{co} \equiv F_c/F_{tf}$, the catalyst:oil ratio. The droplet heat-up rate is dictated by the balance between heating and cooling. For a single droplet, we have

$$W_f C_{pd}\sum_i x_i \frac{dT}{dt} = h\pi D^2(T_g - T) - \sum_i r_{vi}\,\Delta H_{vi} - \Delta H_c \sum_i r_{ci} \tag{6}$$

where h, ΔH_{vi}, and ΔH_c are the heat transfer coefficient, heat of resid vaporization, and heat of resid thermolysis, respectively.

When the droplet reaches the bubble point T_{bp}, the above equation becomes

$$\sum_i r_{vi}\,\Delta H_{vi} + \Delta H_c \sum_i r_{ci} = h\pi D^2(T_g - T_{bp}) \tag{7}$$

It follows that

$$r_{vi} = \frac{x_i}{\sum_i x_i}\sum_i r_{vi} = \frac{x_i}{\sum_i x_i\,\Delta H_{vi}}\sum_i r_{vi}\,\Delta H_{vi} \tag{8*}$$

The initial conditions at $t = 0$ are as follows:

$$x_i = x_{if}, \qquad T = T_f \tag{9*}$$

Note that $\sum_i x_{if} = x_{df}$. Prior to the heating of the resid droplet, the system instantaneously reaches a thermal equilibrium at the base of the riser, which gives the following initial condition for T_g:

$$t = 0, \quad T_g = \frac{R_{co}C_{pc}T_{rg} + x_s C_{ps}T_s + \delta(1 - x_{df})(C_{pl}T_{gf} - \Delta H_{gv})}{R_{co}C_{pc} + x_s C_{ps} + (1 - x_{df})C_{po}\delta} \tag{10*}$$

2.3. Momentum balance

To calculate the heat and mass transfer coefficients, we need to estimate the droplet Reynolds number Re. We consider only the droplet's axial velocity and neglect the influence of flowing catalyst. Let v be the drop-gas slip velocity, i.e. $v = u_g - u_d$, where u_g and u_d are gas and drop velocities, respectively. For simplicity, only the drag, gravitational, and buoyancy forces are considered. The rate of change of axial momentum reads

$$\frac{d(Wu_d)}{dt} = \frac{\pi}{8}D^2\rho_g v|v|C_D - \frac{1}{6}\pi D^3 g(\rho_d - \rho_g) \tag{11*}$$

where W, ρ_d, and ρ_g are the mass of the drop, the drop density, and the gas density, respectively. The drag coefficient C_D is a function of $Re = \rho_g D v/\mu_g$ with μ_g being the gas viscosity.

As mentioned, we assume that the droplet quickly decelerates to its terminal velocity v_t before significant heat transfer takes place. That is, over the time scale for heat transfer, the droplet is at kinematic equilibrium with the surrounding gas. Setting $d(Wu_d)/dt = 0$ gives v_t; i.e.

$$v_t = \sqrt{\frac{4gD_f(\rho_{df} - \rho_g)}{3\rho_g C_D}} \tag{12}$$

where D_f and $\rho_{df} = 1/(\sum x_{if}/\rho_i)$ are the initial drop diameter and average density, respectively. C_D is a function of v_t through the following standard correlation $C_D = b/Re^n$ [10]. Table 1 gives the values of b and n, both of which depend on Re. Note that we have neglected the influence of evaporation on C_D. Evidently, to calculate v_t one needs to simultaneously solve Eq. (12) and $C_D = b/Re^n$ through trial and error. To avoid this laborious procedure, we

Table 1
Values of b and n for different flow regimes

Regime	Re	G	b	n
Stokes	<2	<3.3	24	1
Intermediate	2–500	3.3 ~ 43.6	18.5	0.6
Newton	500 to 2×10^5	>43.6	0.44	0

define the following readily calculable dimensionless quantity G defined as $G \equiv D_f[g\rho_g(\rho_{df} - \rho_g)/\mu_g^2]^{1/3}$. As shown in Table 1, from G one can obtain the corresponding b and n, which in turn give v_t by

$$v_t \equiv \alpha_g u_g = \left[\frac{4gD_f^{1+n}(\rho_{df} - \rho_g)}{3b\mu_g^n \rho_g^{1-n}}\right]^{1/(2-n)} \quad (13)$$

where the slip factor α_g ($0 \le \alpha_g \le 1$) is a measure of the extent of drop-gas slip. The above equation also shows v_t as a function of drop size. We next determine α_g for Cases A and B.

Case A: Here the gas phase comprises steam only. Changing the subscript from g (gas) to s, we calculate the drop–steam slip factor α_s as follows:

$$\alpha_s = \frac{v_{ts}}{u_s} = \frac{A\rho_s v_{ts}}{F_{tf}x_s(1 + (\rho_s x_{df}/x_s\rho_{df}) + \rho_s R_{co}/\rho_c x_s)} \quad (14)$$

The steam density is $\rho_s = 18P_{rb}/[RT_g(0)]$, where A is the riser's cross-sectional area and P_{rb} the pressure at the riser bottom.

Case B: Since, in this case the gas phase essentially comprises gas–oil, we change the subscript from g to o. The drop-gas–oil slip factor α_o can then be calculated by

$$\alpha_o = \frac{v_{to}}{u_o} = \frac{A\rho_o \varepsilon v_{to}}{F_{tf}(1 - x_{df} + x_s)} \quad (15)$$

where the riser void fraction ϵ is given by

$$\varepsilon = \frac{1 - x_{df} + x_s}{1 - x_{df} + x_s + \rho_o x_{df}\sum_i x_{if}/\rho_i + (\rho_o/\rho_c)R_{co}} \quad (16)$$

2.4. Constitutive relations and correlations

The thermolysis rate r_{ci} in the liquid phase is first order, that is

$$r_{ci} = k_i W_f(x_i - \lambda_i x_{fi}) \ge 0 \quad (17)$$

where $\lambda_i = 0$ except for the >1235 °F fraction for which $\lambda_i = 0.3$. This says that only 70% of the >1235 °F fraction is crackable. The rate constant k_i takes the usual Arrhenius form $k_i = k_{oi}\exp(-E_i/RT)$, with $E_i = 50$ kcal/mol for every i. The rate of evaporation, r_{vi}, driven by departure from equilibrium, takes the form as follows:

$$r_{vi} = k_x \pi D^2 \left(\frac{x_i}{\sum_j x_j/M_j} - \frac{M_i y_i}{K_i}\right) \quad (18)$$

The heat and mass transfer coefficients, h and k_x, are calculated from standard correlations in terms of the Nusselt number (Nu) and the Sherwood number (Sh), respectively [11], as follows:

$$Nu = 2 + 0.6Re^{1/2}Pr^{1/3} \quad (19)$$

$$Sh = 2 + 0.6Re^{1/2}Sc^{1/3} \quad (20)$$

In which $Sh = k_x D/(D_{rg}C_t)$, $Nu = hD/k_g$, $Re = Dv_g\rho_g/\mu_g$, $Sc = \mu_g/(D_{rg}\rho_g)$, and $Pr = C_{pg}\mu_g/k_g$. Here, Sc and Pr are the Schmidt number and Prandtl number, respectively.

The total vapor concentration at the droplet surface c_t is calculated by the ideal gas law,

$$c_t = \frac{P_{rb}}{R[0.5(T + T_g)]} \quad (21)$$

The distribution coefficients K_i are expressed as a fourth degree of polynomial function of temperature as follows:

$$\boldsymbol{K} = \max(0, \boldsymbol{BT}) \quad (22)$$

The components of these vectors and matrix are: $\boldsymbol{K}^T = \{K_0, K_1, K_2, K_3, K_4, K_5\}$, $\boldsymbol{T}^T = \{1, T, T^2, T^3, T^4\}$, and

$$\boldsymbol{B} = \begin{bmatrix} -62.2254 & 0.191562 & -2.16982 \times 10^{-4} & 1.0632 \times 10^{-7} & -1.87411 \times 10^{-11} \\ 0.708463 & -0.0106431 & 2.36872 \times 10^{-5} & -1.89383 \times 10^{-8} & 5.15493 \times 10^{-12} \\ 18.4828 & -0.0665283 & 8.88024 \times 10^{-5} & 5.21796 \times 10^{-8} & 1.14058 \times 10^{-11} \\ 26.65 & -0.0922392 & 1.18662 \times 10^{-4} & -6.72804 \times 10^{-8} & 1.141944 \times 10^{-11} \\ 47.2984 & -0.153606 & 1.86122 \times 10^{-4} & -9.97305 \times 10^{-8} & 1.99421 \times 10^{-11} \\ -9.00024 \times 10^3 & 21.4484 & -0.0191645 & 7.60768 \times 10^{-6} & -1.13175 \times 10^{-9} \end{bmatrix}$$

For simplicity, we assume that T_{bp} depends on x_i and the average normal boiling point (NBP) T_{bi} in the following simple fashion:

$$T_{bp} = \frac{\sum_i (x_i/M_i)T_{bi}}{\sum_i (x_i/M_i)} \quad (23)$$

As Table 2 shows, the droplet is quite heavy in that it contains 43.4 wt.% of the >1235 °F material. Also included in the table are each boiling fraction's average NBP, average molecular weight, thermolysis rate constant k_i at 1000 °F (provided by Dr. I.A. Wiehe of our laboratory), and heat of vaporization ΔH_{vi}.

Finally, the mole fraction of each of the resid boiling fractions in the vapor phase is given by:

$$y_i = \frac{x_{vi}/M_i}{(x_o - \sum_j x_{vj})/M_{go} + \sum_j x_{vj}/M_j + x_s/18} \quad (24)$$

3. Results

Calculations were performed for each of the two limiting cases. The inlet conditions are: $T_{rg} = 1235$ °F, $x_{df} = 20$ wt.%, $x_s = 5$ wt.%, feed steam temperature = 291 °F,

Table 2
Properties of resid pseudocomponents

Resid component	Concentration (wt.%)	NBP (°F)	MW (lb/lb mol)	k_i (1000 °F) (s^{-1})	ΔH_{vi} (Btu/lb)
<1050 °F	12.74	900	430	0	70
1050–1090 °F	10.73	1070	650	0.132	62
1090–1150 °F	13.09	1120	740	0.164	61
1150–1200 °F	12.57	1175	860	0.180	60
1200–1235 °F	7.50	1222	980	0.196	60
>1235 °F	43.37	1368	1460	0.228	60

feed temperature $T_{gf} = T_f = 600$ °F, catalyst:oil ratio (R_{co}) = 5 (based on the total hydrocarbon feedstock), hydrocarbon feed flow rate (F_{tf}) = 150 lb/s, riser base pressure = 3 atm. The thermophysical parameters were obtained at an average temperature (1050 °F for the gas oil and 1100 °F for the resid).

3.1. Case A: high temperature environment

Calculations were done for the following initial droplet diameters: 60, 200, 400, 600, 1000 and 1200 μm. To see the relative importance of evaporative versus thermolytic cooling, for each drop size, we made three sets of calculations corresponding to: (1) heating in the presence of both thermolysis and evaporation; (2) heating in the presence of thermolysis only; (3) heating in the presence of evaporation only. To facilitate the discussion, let us imagine there are two switches that can be independently turned on and off: one, for thermolysis and the other, for evaporation.

We begin by looking at the 60 μm droplet. The lower solid curve as shown in Fig. 2 shows its temperature history when evaporation and thermolysis both are operative. This tiny droplet in 28 ms attains its wet-bulb temperature of 1134 °F, which is about 114 °F cooler than the surrounding gas. During the 28 ms heat-up period, neither evaporative nor thermolytic cooling is important mainly because the drop temperature is not sufficiently high. In consequence, during this period the droplet size remains essentially constant, as depicted in Fig. 3, which plots $(D/D_f)^2$ versus t. The droplet, with a total lifetime of about 45 ms, spends slightly more time in transient heat-up than in size shrinkage. After the heat-up period, the D^2-law can adequately describe the size shrinkage caused by evaporation. Thermolysis cannot be important during the extremely short life of this tiny drop (which has a large surface:volume ratio). In fact, Fig. 2 indicates that as long as evaporative cooling operates, one obtains basically the same temperature history (dotted curve) whether thermolytic cooling is present or not. On the other hand, if one switches off evaporative cooling while keeping thermolytic cooling, the droplet temperature (dashed curve) continues to increase and eventually approaches the gas temperature after a long time (ca. 387 ms). Essentially, the life of this small droplet can be divided into two stages. The early stage is sensible heating without evaporative loss. This is followed by evaporation until the droplet vanishes. The gas temperature changes slowly as far as the droplet is concerned, justifying the assumption of gas-phase quasi-steadiness.

The importance of thermolytic cooling should grow with increasing droplet size. Fig. 4 depicts the temperature history for the 200 μm drop. As in the previous case, the lower

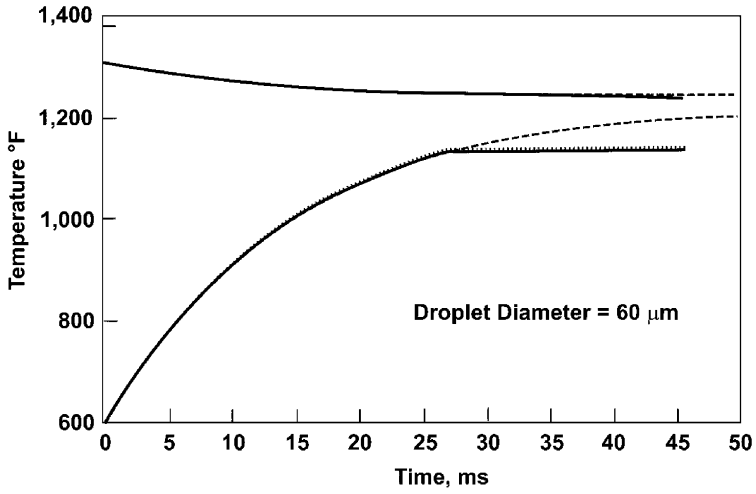

Fig. 2. Temperature history for 60 μm drop, Case A: solid curve, both thermolysis and evaporation are operative; dotted curve, only evaporation is operative; dashed curve, only thermolysis is operative.

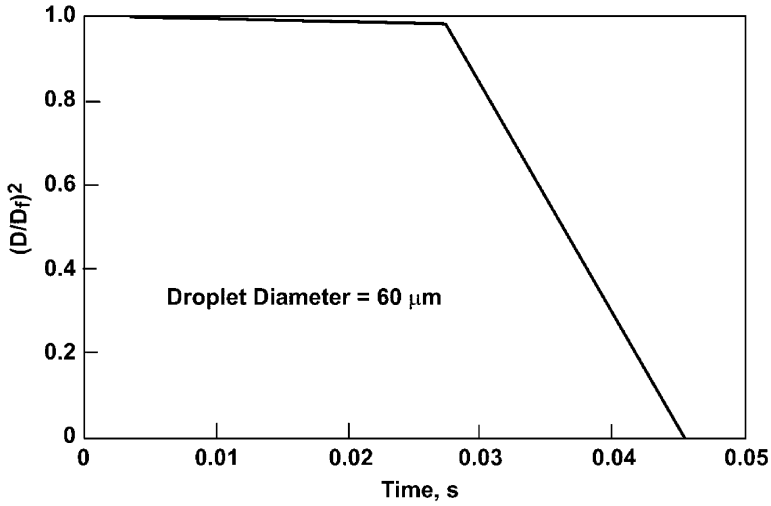

Fig. 3. D^2-plot for 60 μm drop, Case A.

solid curve is for simultaneous thermolytic and evaporative cooling. The droplet takes about 0.25 s to reach its wet-bulb temperature of 1129 °F which is well below the gas temperature of 1247 °F. The total lifetime of the droplet is about 0.41 s (as shown in Fig. 5 also). If one switches off the thermolytic cooling while keeping the evaporative cooling, the droplet temperature attains a higher wet-bulb temperature in about 0.23 s (dotted curve). On the other hand, if the thermolytic cooling is operative while the evaporative cooling is not, the droplet steadily approaches (dashed curve) the gas temperature of 1236 °F after about 1.16 s (not shown) with $D/D_f = 0.64$. Fig. 5 is the corresponding D^2-law plot which can be characterized by three regions. In the early time region (say, up to $t = 0.14$ s), corresponding to the transient heat-up, the droplet size hardly changes. In the intermediate time region (say, $0.14 < t < 0.24$ s), the droplet size changes slowly, mainly due to thermolysis. In the late time region ($t > 0.24$ s), evaporative cooling predominates and the D^2-law provides a good approximation. Evaporative cooling is a stronger driving force than thermolytic cooling for drop shrinkage.

As Figs. 6 and 7 show, the results for the 400 μm droplet are qualitatively similar to those as shown in Figs. 4 and 5. Here, again thermolytic cooling kicks in earlier than evaporative cooling. This droplet has a lifetime of about 1.26 s. The effects of evaporative and thermolytic cooling are comparable to each other, Fig. 6.

Depicted in Fig. 8 are the results for an even bigger drop of 600 μm. This droplet has a lifetime of about 2.2 s which is comparable to the vapor residence time in a typical short contact time riser. Here, the effect of thermolytic cooling becomes more pronounced than the previous case.

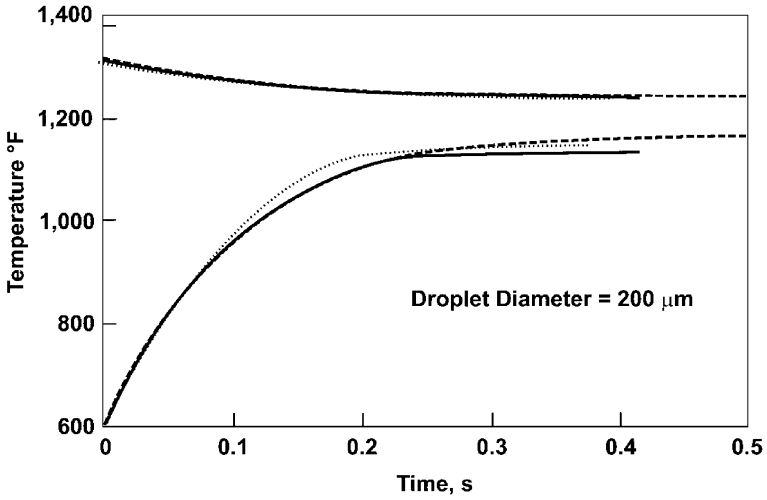

Fig. 4. Temperature history for 200 μm drop, Case A: solid curve, both thermolysis and evaporation are operative; dotted curve, only evaporation is operative; dashed curve, only thermolysis is operative.

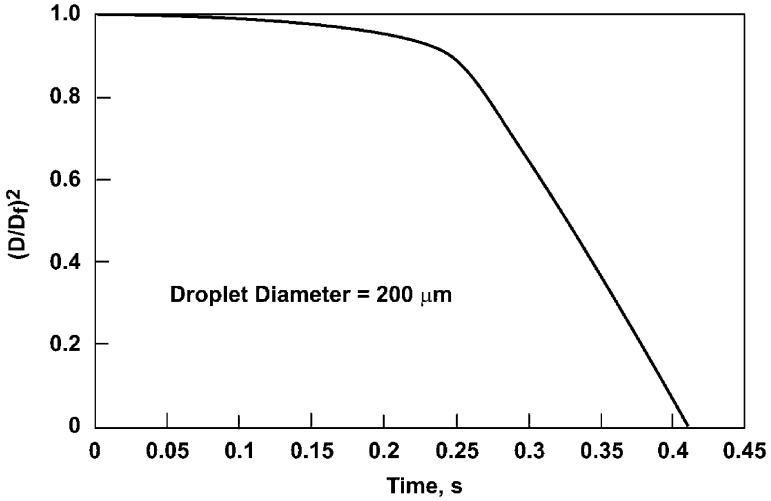

Fig. 5. D^2-plot for 200 μm drop, Case A.

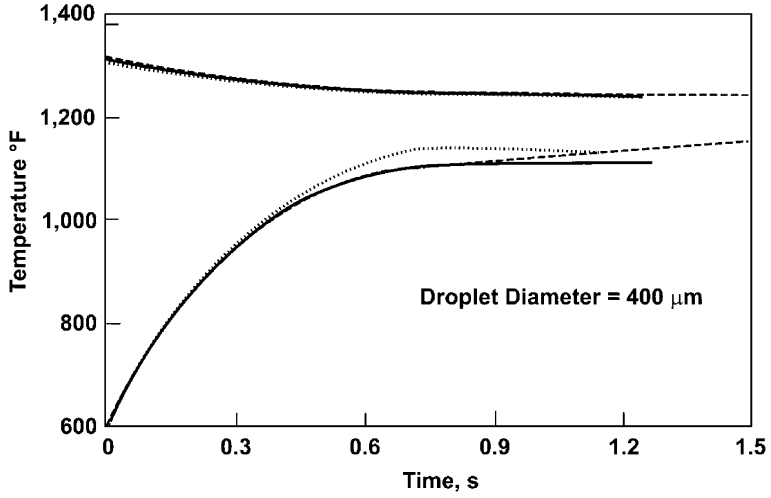

Fig. 6. Temperature history for 400 μm drop, Case A: solid curve, both thermolysis and evaporation are operative; dotted curve, only evaporation is operative; dashed curve, only thermolysis is operative.

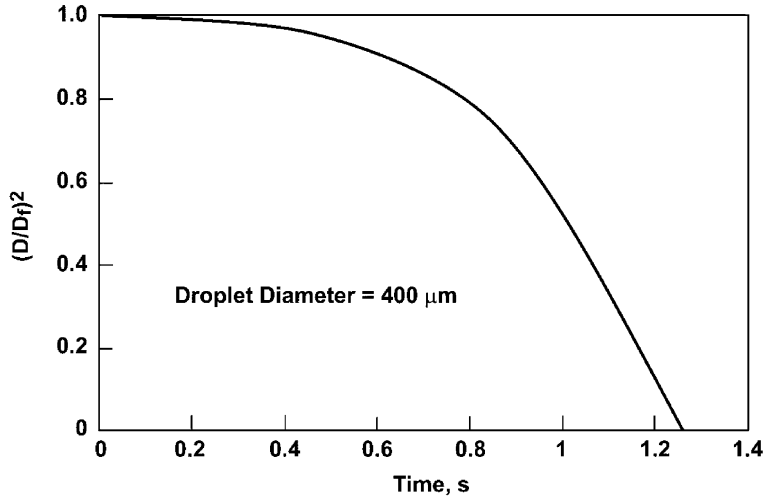

Fig. 7. D^2-plot for 400 μm drop, Case A.

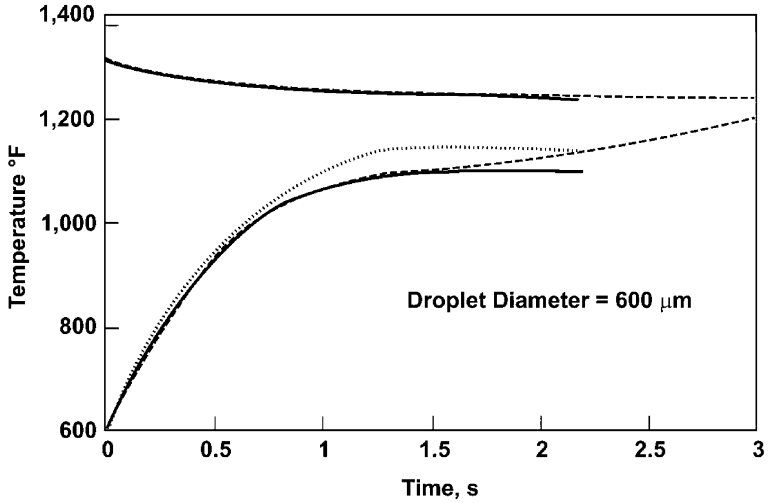

Fig. 8. Temperature history for 600 μm drop, Case A: solid curve, both thermolysis and evaporation are operative; dotted curve, only evaporation is operative; dashed curve, only thermolysis is operative.

The absence of thermolysis raises the wet-bulb temperature by about 40 °F. The D^2-law plots as shown in Fig. 9 for different drop sizes indicate that thermolysis becomes increasingly important with increasing drop size. As an aside, we remark that at the same flow conditions inside the feed injector, the drop size of resid is larger than that of gas oil due to resid's higher viscosity and surface tension.

Figs. 10 and 11 show the temperature histories for the 1000 and 1200 μm droplets whose wet-bulb temperature are 1082 and 1079 °F, respectively. With their lifetimes being 4.1 and 5.0 s, neither droplet would undergo substantial vapor-phase cracking in a present-day short contact time FCC riser. As shown by the dotted curves, the absence of thermolysis raises the wet-bulb temperature by almost 58 and 62 °F for the 1000 and 1200 μm droplets, respectively. Evaporation effect becomes apparent only toward the late stages of the drop life. The temperature history (dashed curve) in the presence of thermolysis only is concave downward initially and then becomes concave upward at large times (as also shown in Figs. 6 and 8). This results from enhanced gas-to-droplet heat transfer, leading to a faster approach to the equilibrium temperature.

3.2. Case B: low temperature environment

Here, pre-vaporization of the gas oil and steam causes a substantial reduction in the catalyst temperature, from 1325 to 1049 °F. Relative to Case A, the catalyst has less heat to give to the droplet. At this low initial temperature, the vapor pressures of the boiling fractions are so low that the cooling

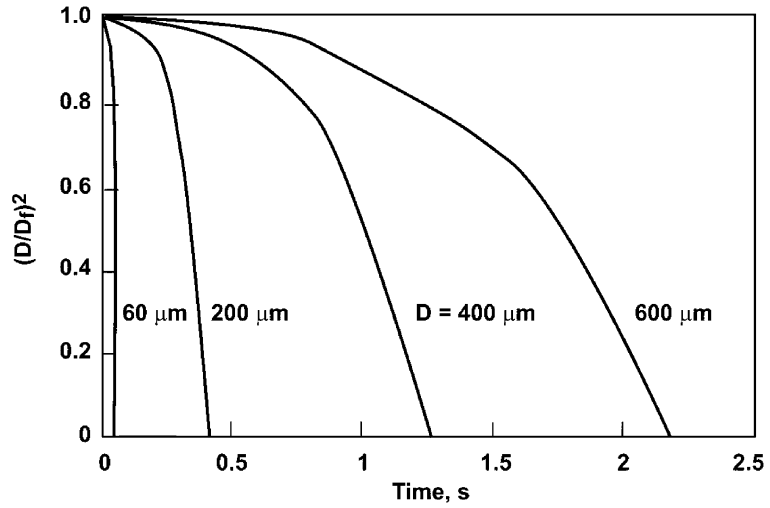

Fig. 9. D^2-plots for 60, 200, 400, 600 μm drops, Case A.

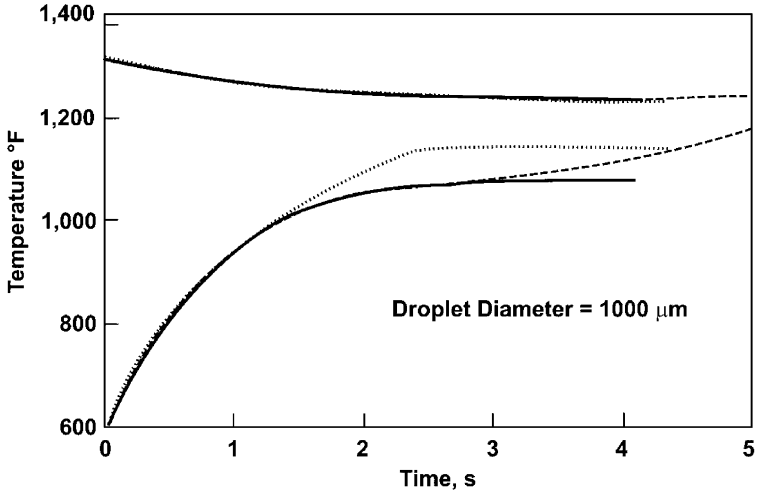

Fig. 10. Temperature history for 1000 μm drop, Case A: solid curve, both thermolysis and evaporation are operative; dotted curve, only evaporation is operative; dashed curve, only thermolysis is operative.

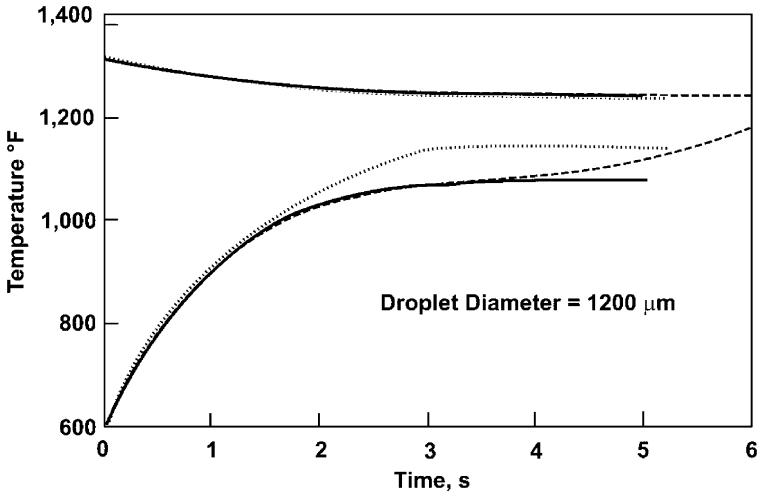

Fig. 11. Temperature history for 1200 μm drop, Case A: solid curve, both thermolysis and evaporation are operative; dotted curve, only evaporation is operative; dashed curve, only thermolysis is operative.

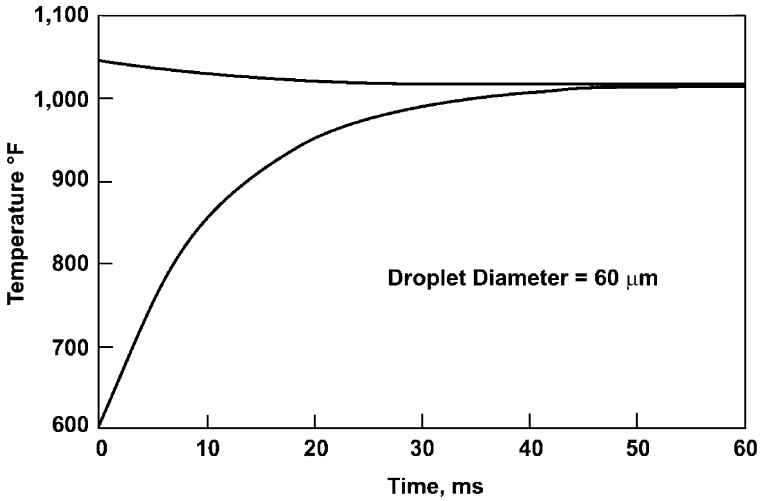

Fig. 12. Temperature history for 60 μm drop, Case B: neither evaporation nor thermolysis is important.

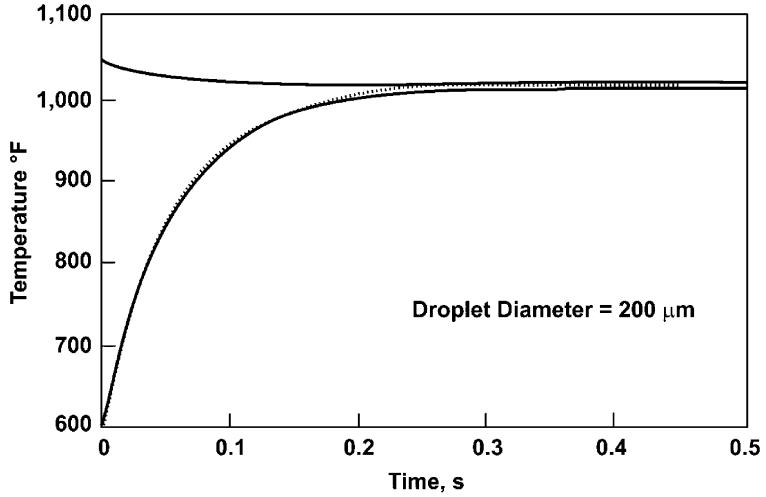

Fig. 13. Temperature history for 200 μm drop, Case B: solid curve, both thermolysis and evaporation are operative; dotted curve, only evaporation is operative.

effect of evaporation is negligibly small for all practical purposes. Consequently, the situation here is less eventful than Case A.

Fig. 12 shows the temperature history of the 60 μm droplet. Neither thermolysis nor evaporation is important; the droplet's life is essentially governed by sensible heating only. After 60 ms, the droplet and gas essentially reach thermal equilibrium. In the absence of evaporation, the extent of size shrinkage at equilibrium under the same conditions should be the same for all drop sizes, the only difference being the time required to attain the equilibrium state (defined here as the state where the gas–drop temperature difference is within 1 °F). The degree of droplet shrinkage at equilibrium, measured by $(D_e/D_f)^2$ where D_e is the drop diameter at equilibrium, is 0.963. Virtually the same result, $(D_e/D_f)^2 = 0.966$, was obtained in the absence of thermolysis. Thus, the majority of the drop's constituents will not vaporize even after a long time. For instance, after 287 ms with both thermolysis and evaporation present, the gas and droplet temperatures are 1014.7 and 1013.8 °F, with $(D/D_f)^2 = 0.85$.

As Fig. 13 shows, the behavior of the 200 μm droplet is very similar to that of the 60 μm droplet in that the life of the droplet for all practical purpose goes through only the sensible heating stage. For $t = 0.5$ and 5 s, the corresponding $(D/D_f)^2$ are 0.892 and 0.367, respectively.

The dotted curve in Fig. 14 represents the case, where thermolysis is switched off for the 400 μm droplet. The difference between solid and dashed curves reflects the effect of thermolysis. The wet-bulb temperature would have been

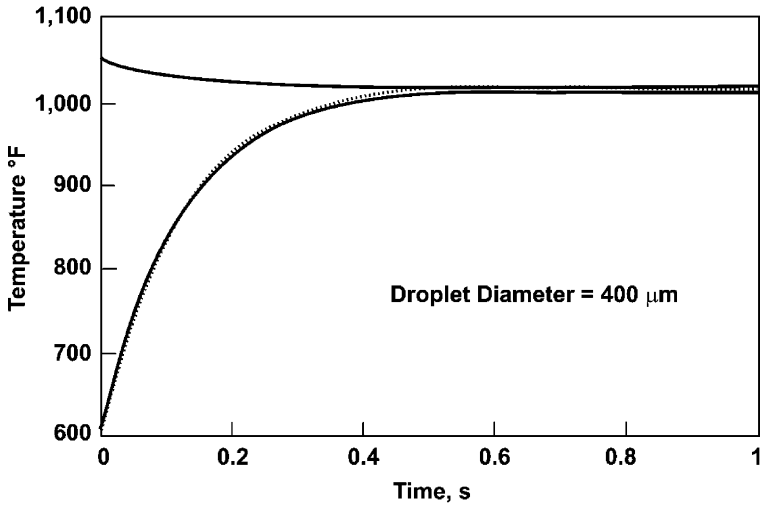

Fig. 14. Temperature history for 400 μm drop, Case B: solid curve, both thermolysis and evaporation are operative; dotted curve, only evaporation is operative.

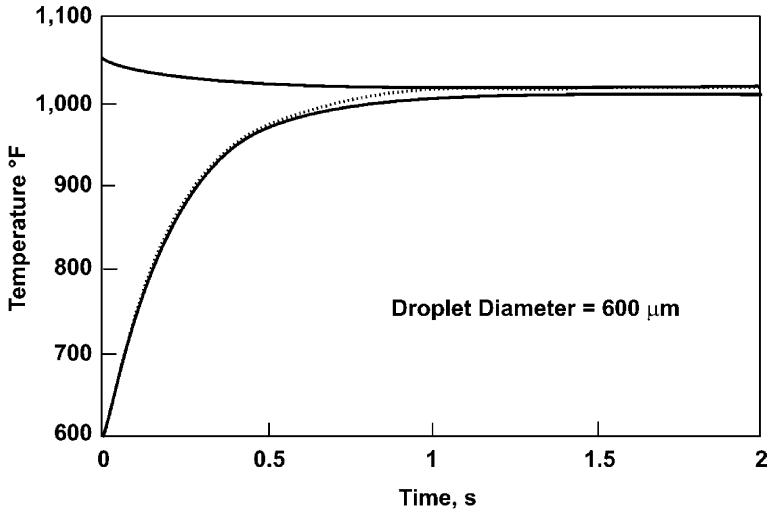

Fig. 15. Temperature history for 600 μm drop, Case B: solid curve, both thermolysis and evaporation are operative; dotted curve, only evaporation is operative.

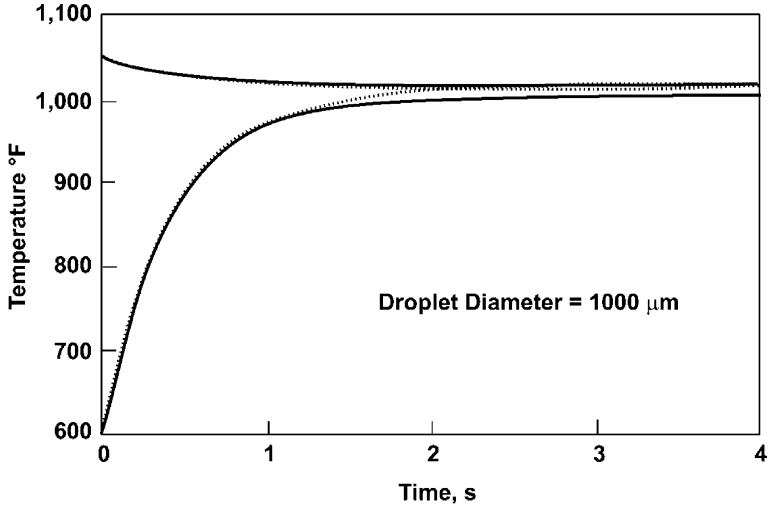

Fig. 16. Temperature history for 1000 μm drop, Case B: solid curve, both thermolysis and evaporation are operative; dotted curve, only evaporation is operative.

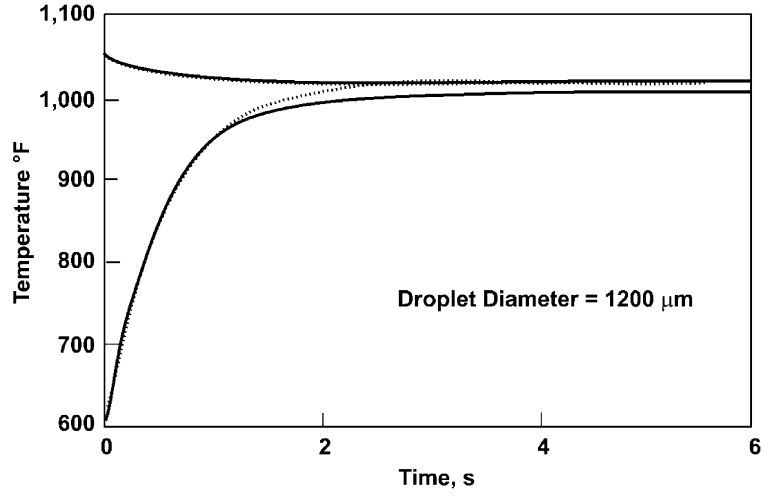

Fig. 17. Temperature history for 1200 μm drop, Case B: solid curve, both thermolysis and evaporation are operative; dotted curve, only evaporation is operative.

5 °F higher had it not been for thermolysis. At $t = 1$ s, $(D/D_f)^2 = 0.852$; this value would have been 0.935 if not for evaporation.

Figs. 15–17 show the slow heat-up rates for the 600 to 1200 μm droplets. The effect of thermolysis on droplet's wet-bulb temperature increases with droplet size, but the magnitude of the effect is much smaller than that in Case A. This is hardly surprising given the high activation energy of the thermolysis reaction.

4. Conclusions

Heavy feed FCC plays an increasingly important role in fuels manufacturing. In light of this, we have developed a simple model that describes how a resid droplet vaporizes as a result of the interplay of interfacial heat and mass transfer, thermal cracking, and gas–drop slip in FCC. Key findings from the model are summarized as follows.

(1) Vaporization of the droplet can go through one to three stages (heat-up, thermolysis, and evaporation), depending on initial drop size and environment. (2) During evaporation, the drop surface area decrease can be approximated by the classical D^2-law. (3) Thermolysis can significantly lower the drop's steady-state temperature—the larger the drop, the greater the effect and hence the longer the drop lifetime. The implication is that large drops may not completely vaporize in the riser, thus, resulting in wicking of the liquid into catalyst pores. Incomplete vaporization can increase coke yield arising from the long liquid residence (soak) time inside the catalyst.

Due to the simplifying assumptions used in the model, the above results should be used only as a qualitative guide on a relative basis. Future studies should extend the present theory to a variety of FCC feeds and should relax some of the assumptions used in the present study.

Acknowledgements

Z. Huang acknowledges the support of a summer internship.

Appendix A. Oil internal circulation

This Appendix attempts to answer the question of whether gas flow can induce significant circulation within oil droplets. Internal convective flow can enhances heat and mass transfer to the extent that the composition and temperature within the droplet are spatially uniform but temporally varying.

On the basis of the boundary–layer theory, we obtain an order-of-magnitude estimate of the drop internal velocity induced by external gas flow. Let v_∞ be the main stream–gas velocity relative to a droplet of diameter D. We suppose that the gas exerts enough drag to induce a velocity v_l on the liquid surface. The system under consideration is characterized by the following dimensionless groups: gas Reynolds number, $Re_g = \rho_g v_\infty D/\mu_g$; oil Reynolds number, $Re_l = \rho_l v_l D/\mu_l$; oil thermal Peclet number, $Pe_h = Re_l Pr_l$; oil mass Peclet number, $Pe_m = Re_l Sc_l$. The subscripts l and g signify liquid and gas, respectively.

We look at a conservative case in which the droplet's resistance to internal circulation is still relatively strong (high viscosity). To do so, we consider that the drop is in its early life, so its temperature is relatively low. In the absence of significant volume expansion due to vaporization and cracking, the gas velocity is relatively low. We suppose that there are two viscous boundary layers; one in the gas phase with thickness δ_g, the other inside the oil drop with thickness δ_l.

Now consider the case $T = 800$ °F, $v_\infty = 25$ ft/s, and $D = 400$ mm. The gas flow is laminar, with $Re_g \approx 1500$. In the absence of Marangoni flow, an approximate statement of the continuity of shear stress at the interface is:

$$\mu_g \frac{v_\infty - v_l}{\delta_g} \approx \mu_l \frac{v_l}{\delta_l} \tag{A.1}$$

The result for flat-plate laminar boundary layer flow [10,11] can be used to estimate δ_g and δ_l; that is, $\delta_g \sim DRe_g^{-1/2} = [(\mu_g D)/(\rho_g v_\infty)]^{1/2}$ and $\delta_l \sim DRe_l^{-1/2} = [(\mu_l D)/(\rho_l v_l)]^{1/2}$. From these and assuming that $v_\infty \gg v_l$ yield the internal:external velocity ratio as a function of only fluid properties:

$$\frac{v_l}{v_\infty} \approx \left(\frac{\rho_g \mu_g}{\rho_l \mu_l}\right)^{1/3} \tag{A.2}$$

This ratio increases with temperature. We next look at gas oil and resid droplets separately.

For gas oil drops, $\mu_l \sim 0.3$ cp and $\rho_l \sim 0.67$ g/cm^3, we have $v_l/v_\infty \sim 5.4\%$. For resid drops, $\mu_l \sim 1.78$ cp and $\rho_l \sim 0.78$ g/cm^3, then $v_l/v_\infty \sim 2.8\%$. These results indicate that the induced surface velocity can be of the order of 3–5% of the external gas velocity. Note that the internal velocity v_l increases as the drop gets "older" because of higher temperature. For instance, at 1000 °F $v_l/v_\infty \sim 6.6\%$ for gas oils and $v_l/v_\infty \sim 3.8\%$ for resids.

The thermal Peclet number, Pe_h, tells us the relative magnitudes of the convective versus diffusive heat transfer. To get a conservative estimate of Pe_h, we consider $v_\infty = 10$ ft/s at 800 °F. For a drop of 400 μm diameter, the corresponding liquid Re for gas oils and resids are, respectively, $Re_{l,go} \sim 140$ and $Re_{l,resid} \sim 15$.

Flows of heavy oils are generally characterized by large Pr. At FCC conditions, C_p and k are nearly the same for gas oils and resids. At 800 °F, $Pr \sim 13$ for gas oil drops and $Pr \sim 77$ for resid drops. The corresponding thermal Peclet numbers are $Pe_h \sim 1860$ for gas oil drops and $Pe_h \sim 1155$ for resid drops. These high Peclet numbers suggest that convective flow inside the drops plays the dominant role in the heat transfer. The same is true of mass transfer, since

the liquid phase Schmidt number is generally larger than the Prandtl number and, hence, $Pe_m > Pe_h$.

References

[1] P.B. Venuto, E.T. Habib, Fluid Catalytic Cracking with Zeolite Catalysts, Marcel Dekker, New York, 1979.
[2] J.S. Buchanan, Analysis of heating and vaporization of feed droplets in fluidized catalytic cracking risers, Ind. Eng. Res. Dev. 33 (1994) 3104.
[3] K.N. Theologos, A.I. Lygeros, N.C. Markatos, Feedstock atomization effects on FCC riser reactors selectivity, Chem. Eng. Sci. 54 (1999) 5617.
[4] C. Mirgain, C. Briens, M.D. Pozo, R. Loutaty, M. Bergougnou, Modeling of feed vaporization in fluid catalytic cracking, Ind. Eng. Res. Dev. 39 (2000) 4392.
[5] A. Gupta, D.S. Rao, Model for the performance of a fluid catalytic cracking riser reactor: effort of feed atomization, Chem. Eng. Sci. 56 (2001) 4489.
[6] S.L. Chang, S.A. Lottes, C.Q. Zhou, B.J. Bowman, M. Petrick, Numerical study of spray injection effects on the heat transfer and product yields of FCC riser reactors, Trans. ASME 123 (2001) 544.
[7] J. Gao, J.C. Xu, S. Lin, G. Yang, Y. Guo, Simulation of gas–liquid–solid three-phase flow and reaction in FCC riser reactors, AIChE J. 47 (2002) 677.
[8] K.K Kuo, Principles of Combustion, Wiley, New York, 1986.
[9] T.C. Ho, Study of coke formation in resid catalytic cracking, Ind. Eng. Chem. 31 (1992) 2282.
[10] M. M. Denn, Process Fluid Mechanics, Prentice-Hall, Upper Saddle River, Englewood Cliffs, NJ, 1980.
[11] R.B. Bird, W.E. Stewart, E.N. Lightfoot, Transport Phenomena, Wiley, New York, 1960.